Single-Mode Rayleigh–Taylor Growth-Rate Measurements with the OMEGA Laser System

Understanding the growth of perturbations due to hydrodynamic instabilities is important to the design of direct-drive targets for the National Ignition Facility (NIF). Direct-drive inertial confinement fusion (ICF) has the potential to be more efficient than indirect-drive ICF; however, there is the potential for greater growth of hydrodynamic instabilities due to the lower ablation velocities, which will prevent a NIF target from igniting. The primary instability of concern is the Rayleigh–Taylor (RT) instability, where a less dense fluid "supports" a more dense fluid and as such merits a thorough investigation. Direct-drive targets are subject to the RT instability twice during an ICF target implosion: first during the ablative acceleration phase of the implosion and second when the deceleration phase begins core assembly. Target imperfections and laser-irradiation nonuniformities act as amplitude seeds for the acceleration RT instability, while interior target imperfections and feedthrough of the ablation surface growth to the fuel–pusher interface act as amplitude seeds for the deceleration RT instability.

The importance of the RT instability problem is reflected in the number of experiments conducted[1–5] to determine the RT growth rates in directly driven systems. Experiments of interest have used laser irradiation of 527 nm and 351 nm and have employed a number of beam-smoothing schemes. It is the development of these advanced laser-irradiation smoothing techniques like induced spatial incoherence (ISI)[6] and smoothing by spectral dispersion (SSD)[7] that has enabled the RT growth experiments to yield quantitative data. Without the beam-smoothing techniques, irradiation nonuniformity can dominate the experimental observables, even in initial-large-amplitude, single-mode, mass-perturbation experiments.

The RT growth rate at the ablation surface has typically been described by the Takabe[8] or modified Takabe dispersion formula given by

$$\gamma = \alpha \cdot \sqrt{k \cdot g} - \beta \cdot k \cdot V_a$$

and

$$\gamma = \alpha \cdot \sqrt{\frac{k \cdot g}{1 + k \cdot L}} - \beta \cdot k \cdot V_a ,$$

respectively, where γ is the growth rate, k is the wave number of the perturbation, g is the acceleration of the interface, V_a is the ablation velocity, α is a constant approximately equal to 0.9, β is a constant with an approximate value of 3, and L is the density scale length at the ablation surface. The importance of thermal conduction[9] has been investigated and leads to a modification of the Takabe formula for the growth rate through changes in the values α and β that depend on the details of the thermal transport at the ablation surface.

Details of the dispersion formula for RT growth rates remain an active subject of research at this time. Previous measurements[10] of the growth rate, conducted using x-ray radiography, have yielded values that are substantially lower than that calculated by either of the above formulae. The need for nonthermal electron transport has been proposed as the cause for these lower growth rates.

The results from a series of single-mode RT-instability growth experiments performed on the OMEGA laser system using planar targets are presented. Planar targets with imposed mass perturbations were accelerated using five to six 351-nm laser beams overlapped with a total overlapped intensity up to 2.5×10^{14} W/cm^2. Experiments were performed with both 3-ns ramp and 3-ns flat-topped temporal pulse shapes. The use of distributed phase plates (DPP's)[11] and SSD resulted in a laser-irradiation nonuniformity of 4%–7% over a 600-μm-diam region defined by the 90% intensity contour.

The temporal growth of the modulation in optical depth was measured using through-foil radiography and was detected with an x-ray framing camera. The temporal-growth evolution of the measured variation in the optimal depth for both 31-μm and 60-μm wavelength perturbations was found to be in good agreement with *ORCHID* simulations when the experimental details, including noise, were included. In addition, it has been found that for current experiments care must be taken in

relating the actual ablation-surface RT growth rate from the experimental observables used in these experiments.

Experimental Configuration

A schematic of the experimental layout (Fig. 71.5) shows the orientation of the three foils and diagnostics used in these experiments. The foils are supported by a 140-μm boron-coated carbon fiber. Five to six beams are incident onto the 20-μm-thick CH-foil drive target, which is mounted on a 50-μm-thick Mylar washer with a 1-mm hole in the center. A 2-mm × 2-mm piece of 25-μm-thick uranium is mounted at the other end of the boron-coated carbon fiber 9 mm from the drive foil. Six to twelve beams were used to irradiate the uranium foil in order to generate the x rays needed to radiograph the accelerated foil. A third foil composed of 6-μm-thick aluminum was centered between the drive and backlighter foils to act as a bandpass filter for x rays between 1.0 and 1.5 keV. This prevents the very-low-energy x rays from the uranium target from preheating the accelerated foil.

The typical mass-modulated accelerated foil is composed of a 20-μm-thick CH foil that had perturbations imposed on the side irradiated by the laser. The 20-μm thickness was chosen because it represents about two attenuation depths for the 1.0- to 1.5-keV x rays used for radiography. Perturbation wavelengths of either 31 μm or 60 μm were imposed onto the foils with initial amplitudes of 0.45 μm and 0.5 μm, respectively. The face of the foil irradiated by the laser was overcoated with a 500-Å to 1000-Å layer of Al to prevent shinethrough.[12] (Foils used for acceleration measurements had no initial imposed mass perturbations.)

The primary diagnostic is an x-ray framing camera.[13] The pinhole array is composed of eight 8-μm pinholes arranged in a checkerboard pattern to minimize interference from adjacent images. The framing camera used for the perturbation amplitude measurement has a magnification of 14.1±0.1 with the pinhole array located 24.8 mm from the rear surface of the accelerated foil. A second x-ray framing camera measured the spatial and temporal emissions of the backlighter at a magnification of 6 with a standard 16-pinhole array. Each pinhole is 10 μm in diameter. Data from the backlighter framing camera are shown in Fig. 71.6. The images are timed so that the backlighter reaches full emission in the end of the second strip (i.e., between images 3 and 4). Each image is separated by 50 ps, and the timing of the backlighter emission is known to about 50 ps. The gating pulses for uniform strips of each of the two framing cameras are recorded by an oscilloscope, and the time of each image relative to the drive beams is known to about 100 ps. The temporal resolution of both x-ray framing cameras was 80 ps. The current noise levels on the framing camera allow the instrument to measure perturbations with amplitudes ≥0.4 μm. As a result, the early-time amplitude of the accelerated foils was at the detection limit and, therefore, difficult to resolve.

Laser Irradiation

Typical planar-foil experiments use two independent drivers so that separate pulse shapes could be used for the drive and backlighter beams. The beams were overlapped onto their respective targets with a radial displacement accuracy of 35 μm from the center of each foil.

The backlighter pulse shape used was a 3-ns-wide flat-topped pulse. Each backlighter beam was focused to a 1.5-mm-diam spot at the 5% intensity contour and had an energy of ~400 J for a total of 3.2 to 4.8 kJ on the uranium backlighter.

The two pulse shapes used for the drive beams are shown in Fig. 71.7. The first was a 3-ns ramp pulse, and the second was a 3-ns flat-topped pulse. Each of the drive beams was focused to a ~900-μm-diam spot size (at the 5% intensity contour) and incorporated DPP's with an on-target intensity distribution measured to be $I \propto \exp[-(r/r_0)^4]$. The resultant five- to six-

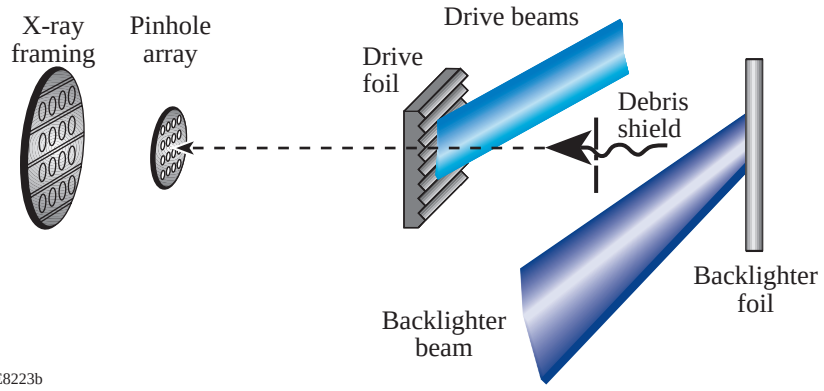

Figure 71.5
Experimental schematic of the target and primary diagnostic. The target is constructed from three foils: a uranium backlighter, an aluminum debris shield, and a CH drive foil with an imposed perturbation. The primary diagnostic is an x-ray framing camera with a 14.1 magnification provided by 8-μm pinholes located 24.8 mm from the accelerated target.

beam overlapped spot had a region of constant intensity of ~600-μm diameter. The drive beams were temporally smoothed by 2-D SSD with a total bandwidth of 0.135 THz at 351 nm with an angular dispersion of 33 μrad/Å × 33 μrad/Å (IR bandwidths of 1.5 Å × 0.7 Å). The total drive intensity for six irradiation beams peaked at 2.5×10^{14} W/cm^2 for the ramp pulse and 2.0×10^{14} W/cm^2 for the flat-topped pulse.

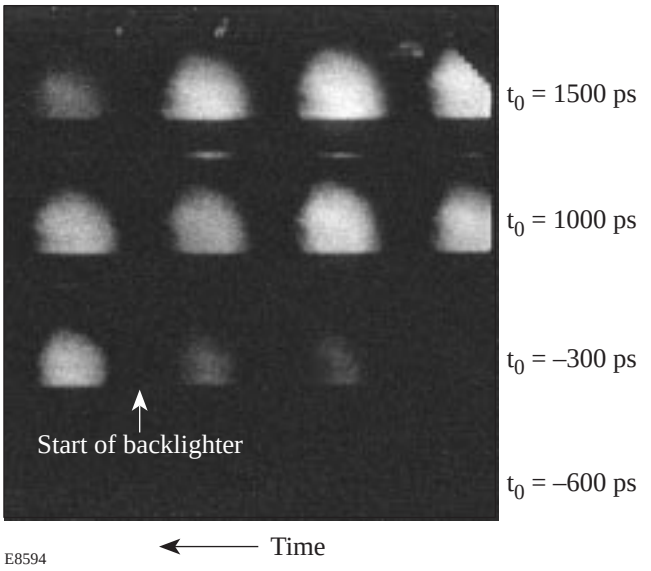

Figure 71.6
Framing camera image of backlighter x-ray emission. The four strips are timed from bottom to top and right to left. The values for t_0 reflect the trigger time of the strip relative to the start of the backlighter pulse.

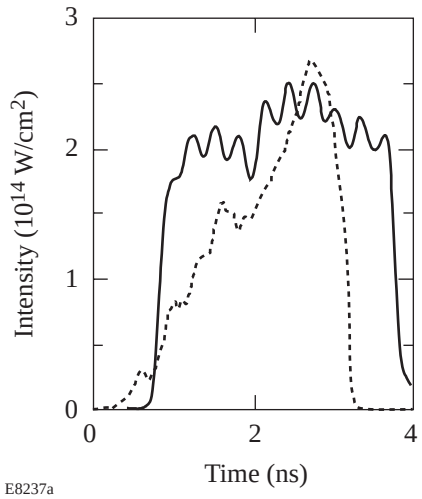

Figure 71.7
Laser illumination pulse shapes used to accelerate the CH target. The 3-ns ramp pulse (dashed curve) has a peak intensity of 2.5×10^{14} W/cm^2, and the 3-ns flat-topped pulse (solid curve) has an intensity of 2.0×10^{14} W/cm^2.

The uniformity of a single beam with a DPP and SSD at the maximum bandwidth for these experiments was measured by imaging the focal spot onto UV-sensitive film and analyzing the intensity distribution.[14] The resultant nonuniformity for a single beam was measured as 12% integrated over ~1 ns. The overlay of six of these beams onto the drive target is, therefore, expected to give an overall nonuniformity of 5%.

Acceleration Measurements

The measured acceleration for a 20-μm-thick CH foil driven with the 3-ns ramp pulse with a peak intensity of 2.5×10^{14} W/cm^2 is shown in Fig. 71.8. The data are shown as squares with error bars that reflect the accuracy of the position measurement. The round points are the position of the foil as simulated by the 1-D hydrodynamics code *LILAC*. The agreement between the measured foil position and the *LILAC* simulation is excellent and shows that the target drive is being accurately modeled.

While the data shown in Fig. 71.8 are consistent with a constant acceleration, the *LILAC* simulation shows that the acceleration (Fig. 71.9) for a 3-ns ramp pulse is not constant and changes by a factor of 2 during the experimental measurement. This points to the importance of complete simulations rather than the application of simplified models that generally assume constant acceleration.

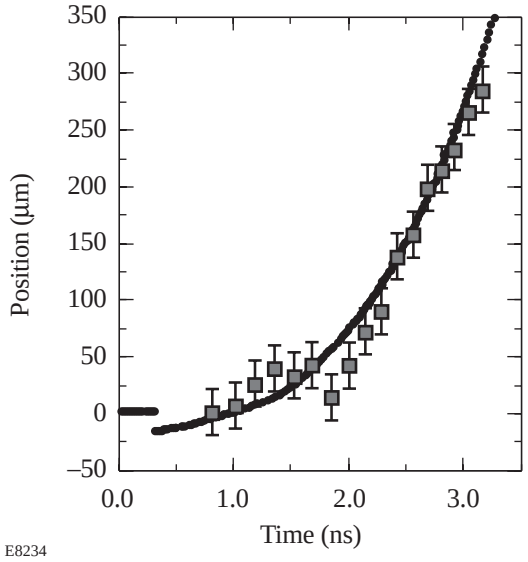

Figure 71.8
Comparison of the measured acceleration of a 20-μm-thick CH foil with a *LILAC* 1-D hydrodynamic simulation. The data are shown as squares with error bars and the calculation as circles.

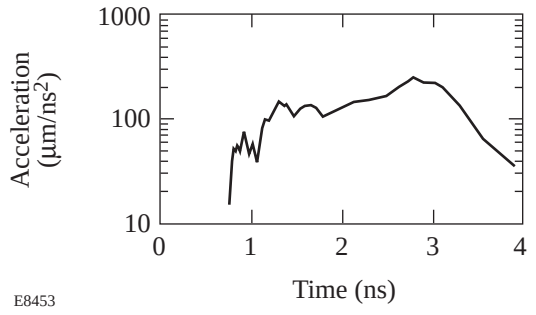

Figure 71.9
The calculated acceleration of a 20-μm-thick CH foil illuminated with a 3-ns ramp pulse with a peak intensity of 2.5×10^{14} W/cm^2. The acceleration predicted by the simulation is not constant in time but continues to increase during the target illumination.

RT Growth Measurements

Face-on radiography was used to measure the RT growth of imposed perturbations. The modulation in the optical depth is calculated by analyzing a 250-μm × 250-μm region of the target for each temporal frame. The backlighter spatial distribution is taken out by fitting a two-dimensional, fourth-order polynomial to the natural log of the intensity. The fourth-order polynomial fit was used to model the x-ray intensity distribution from the backlighter for shots where no drive foil was present. It has also been verified by using higher-order polynomial fits (up to eighth order) and showing no significant improvement in the quality of the polynomial fit as determined from the value of x^2. This fit is then subtracted from the data, leaving the difference. This analysis tacitly assumes that the low-order polynomial adequately models the backlighter emission profile and does not affect the perturbation measurement. The analyzed region for the 31-μm-wavelength perturbation is chosen to be exactly eight wavelengths across the frame. A 2-D Fourier transform (FFT) then yields the optical depth at the perturbation wavelength. One dimension of the FFT is used to measure the imposed perturbation temporal evolution, and the orthogonal direction is used to determine the residual noise in the measurement.

Data from three target shots (plotted in Fig. 71.10) were taken with the 3-ns ramp pulse with a peak intensity of 2.5×10^{14} W/cm^2. The measured data are shown as either diamonds, squares, or triangles. The error bars are calculated by analyzing separate regions in the x-ray images. The results are averaged and the standard deviation is plotted as error bars. The framing camera was triggered at three different times to study the evolution of the perturbation over 2.5 ns. The thick solid line in Fig. 71.10 is the optical depth calculated by the 2-D hydrodynamics code *ORCHID*. It agrees with the measured optical depth late in time but not at early times. The thin solid line is an estimate of the noise in the experimental measurement as determined using the FFT technique outlined above. We thus estimate a minimum measurable optical depth of 0.033 as a noise source. The dashed line in Fig. 71.10 is the sum of the optical depth as calculated by *ORCHID*, and the noise and results are a good fit over the entire measurement time.

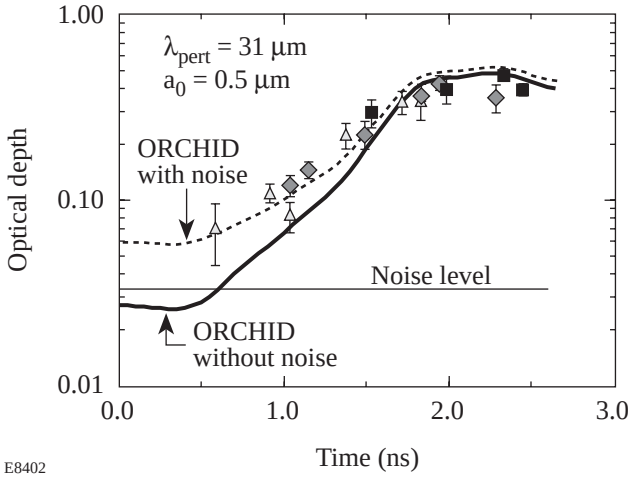

Figure 71.10
A comparison of the experimentally measured optical depth and the predictions of the *ORCHID* 2-D hydrodynamic simulations. Data are shown for three shots as diamonds, squares, and triangles; the calculated optical depth is shown as a solid line. Good agreement with the experimental data is achieved only when the experimental noise is added to the calculated optical depth.

The 3-ns square pulse data are shown in Figs. 71.11(a) and 71.11(b). The growth of an initial perturbation with a wavelength of 60 μm and an initial amplitude of 0.5 μm is shown in Fig. 71.11(a), and the growth of a 31-μm-wavelength perturbation with an initial amplitude of 0.45 μm is shown is Fig. 71.11(b). The data are plotted as points, and the *ORCHID* simulation is plotted as a solid line. In these data the experimental noise has been subtracted from the data before being plotted with the simulation output. Several shots are plotted together so that the temporal development of the modulation in the optical depth can be shown. The agreement between the variation in the optical depth measured with x-ray radiography and the *ORCHID* simulations for both cases is quite good over the temporal range of interest to determining the linear RT growth rate.

The *ORCHID* calculations are a complete end-to-end simulation of the experiment and include the backlighter spectrum,

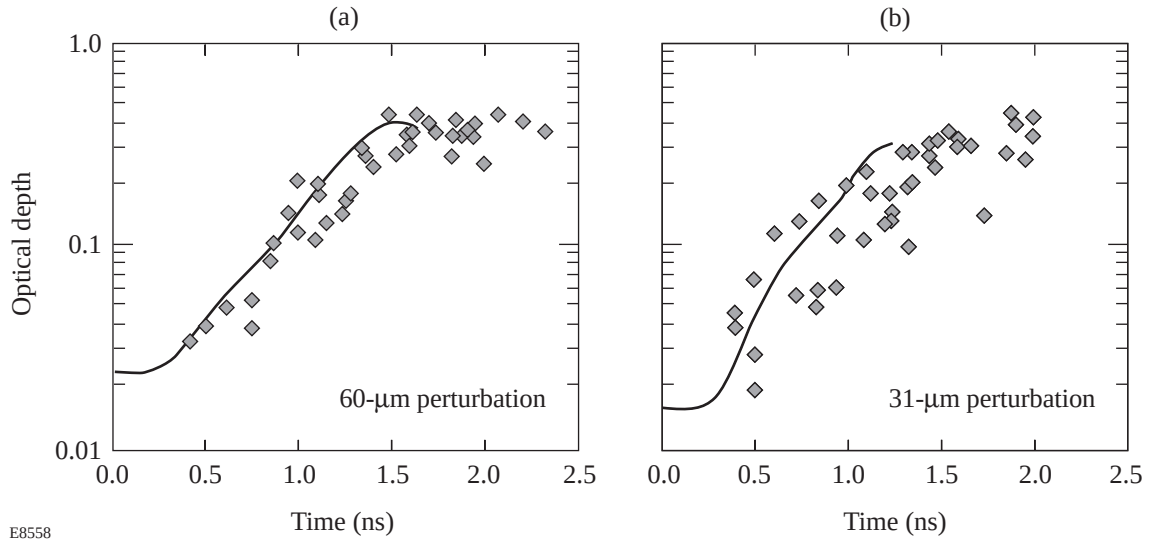

Figure 71.11
A comparison of the experimentally measured optical depth and the predictions of the *ORCHID* 2-D hydrodynamic simulations for both the 60-μm and 31-μm perturbations. Data are shown as diamonds; the calculated optical depth is shown as a solid line. Good agreement with the experimental data is achieved only when the experimental noise is subtracted from the measured optical depth. These are data for a 3-ns square drive pulse.

all filtering of the x-ray framing camera, and a correction for the camera resolution. The comparison of the optical depth calculated from the simulation with the experimental data shows the quality of the simulation. A simple comparison of the growth rate as calculated by a simulation and the growth rate taken from a set of experimental data is not sufficient. Detailed comparisons of the data from a series of planar-foil experiments and their associated numerical simulations show that associating the measured growth rate of the modulation in optical depth with that due to the ablative RT instability must be done with great care, if done at all. During this study, we have identified two important sources of departure in the growth rates inferred from variations in the optical depth as compared to determinations based on variations in the actual displacement at the ablation surface. The first source of discrepancy that must be accounted for is the "noise" in the measurement. Figure 71.10 indicates that using the measured variation in the optical depth yields a growth rate value of 1.6 ns^{-1}, while *ORCHID* (without noise) predicts approximately 2.1 ns^{-1}. Therefore, the accurate determination and treatment of experimental noise are important in determining growth rates. The second, and possibly more important, cause of problems in determining growth rates from the variations in the optical depth has been found to be the initial shock propagation through the foil. The *ORCHID* simulations of these experiments have shown that for the pulse shape–foil combinations used, the shock propagation through the foil has a large influence on the temporal evolution of the modulation in optical depth early in time. The comparison within a given simulation of the growth rate from the evolution of the optical depth with the growth rate determined from the evolution of the ablation surface gives substantially different results. In all cases of large-initial-amplitude mass perturbations considered to date, we have found that the growth rate determined from the modulation in the optical depth is lower than that determined from the modulation in spatial position of the ablation surface (illustrated in Fig. 71.12). Analysis of the *ORCHID* results shows that the propagation of the initial shock through the foil results in a change in the $\rho\Delta x$ of the foil (predominantly through a change in the density) even before the ablation surface has accelerated (or moved) appreciably. A simple approximation to the temporal history of the variation in the $\rho\Delta x$ data has a functional form of $a = a_0 \cdot e^{\gamma t} + \text{constant}$, where the constant is due to the initial shock propagation.

To check this finding one can take the time derivative of $\rho\Delta x$. A closer analysis of the *ORCHID* simulation of a 31-μm-wavelength perturbation is plotted for the time of linear growth (0.8 ns to 1.1 ns) in Fig. 71.13. The data plotted as diamonds are the amplitude of the optical depth of the planar target as determined from the uranium backlighter. The amplitude of the $\rho\Delta x$ at the ablation interface is plotted as squares. The Δx amplitude from the variation in position at the ablation surface is plotted as x's. The growth rate as determined by the $\rho\Delta x$ and

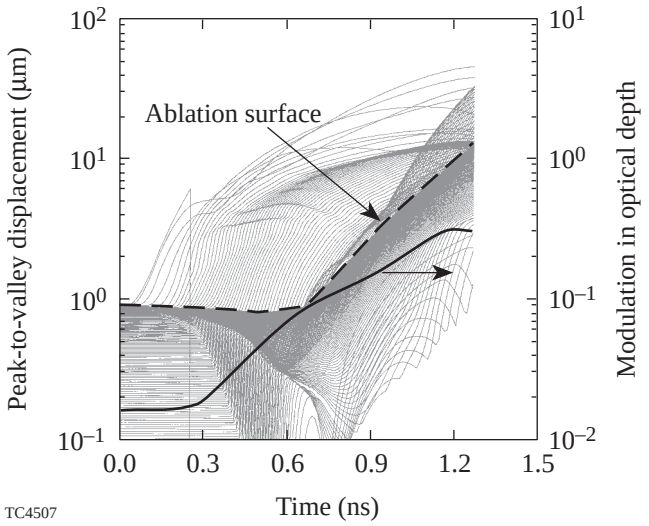

Figure 71.12
ORCHID simulation results for the growth of the perturbation at the ablation surface and the modulation in the optical depth are shown for one of the 31-μm, 0.45-μm initial amplitude experiments.

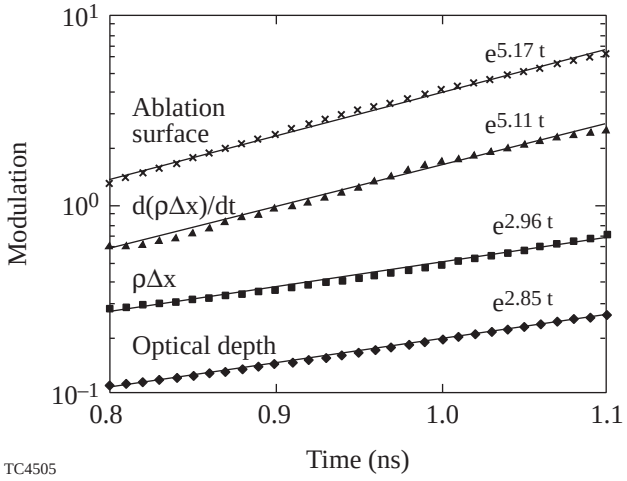

Figure 71.13
The growth of the perturbation as a function of time is plotted for three different simulation quantities: optical depth, $\rho\Delta x$, and ablation-surface amplitude. Both the optical depth and $\rho\Delta x$ show growth rates that are substantially different from the ablation-surface amplitude. The time derivative of $\rho\Delta x$ shows a growth rate that agrees with the ablation-surface amplitude.

the optical depth are in agreement, but there is a significant difference in the growth rates as determined by radiography (optical depth) and the growth rate as determined from the ablation surface. The data plotted as triangles are the time derivative of the amplitude from the $\rho\Delta x$. When the time derivative of $\rho\Delta x$ is taken, the value of γ as determined by the variation in the displacement of the ablation surface is recovered. This behavior was also found for the 60-μm, 0.5-μm-initial-amplitude case and for both pulse shapes considered. (This second reason for growth-rate departures is reminiscent of the experimental noise effect encountered during the analysis of the framing camera data.)

Summary

The OMEGA laser facility has been used to study the growth of perturbations due to the RT instability at the ablation interface. The targets were accelerated with 351-nm illumination at 2.5×10^{14} W/cm^2 for 3-ns ramp pulses and at 2.0×10^{14} W/cm^2 for 3-ns flat-topped pulses. The comparison of target acceleration with 1-D hydrodynamics simulation is good and suggests that the laser drive is correctly modeled. The comparison for the growth of initial perturbations as measured by the change in optical depth agrees with 2-D *ORCHID* simulation when the measurement noise is included. It is important to compare the values of the measured optical depths and not simply the growth rates in order to understand the underlying physics and infer RT growth rates.

The pulse shapes used in our experiments produce both accelerations and ablation velocities that evolve in time. This implies that care must be taken when determining growth rates from experimental data to ensure the validity of the underlying assumptions. The growth rates can be used to compare experimental data for targets with similar perturbations when the temporal region studied coincides with regions where the acceleration and ablation velocity are relatively constant.

It is important that the numerical simulations include as many details associated with the actual experiment and diagnostic configuration as possible. The comparisons between the hydrodynamic simulations and the experimental data should be made with the temporal evolution in optical depth modulation. If good agreement is found between the experimental data and the simulations, then the ablation-surface growth rate as determined from the simulation can be used with some level of confidence, as the RT growth rate for the initial perturbation used in the experiment.

It is evident from the effect of the noise on the comparison with calculations that future experiments will need to address this issue. Instruments and experimental techniques are needed that will reduce the level of noise so smaller initial perturbation amplitudes can be studied. Instruments are also needed that will allow shorter-wavelength perturbations to be studied.

ACKNOWLEDGMENT

This work was supported by the U.S. Department of Energy Office of Inertial Confinement Fusion under Cooperative Agreement No. DE-FC03-92SF19460, the University of Rochester, and the New York State Energy Research and Development Authority. The support of DOE does not constitute an endorsement by DOE of the views expressed in this article.

REFERENCES

1. J. Grun *et al*., Phys. Rev. Lett. **58**, 2672 (1987).
2. M. Desselberger *et al*., Phys. Rev. Lett. **65**, 2997 (1990).
3. S. G. Glendinning, S. V. Weber, P. Bell, L. B. DaSilva, S. N. Dixit, M. A. Henesian, D. R. Kania, J. D. Kilkenny, H. T. Powell, R. J. Wallace, P. J. Wegner, J. P. Knauer, and C. P. Verdon, Phys. Rev. Lett. **69**, 1201 (1992).
4. K. Shigemori *et al*., Phys. Rev. Lett. **78**, 250 (1997).
5. S. G. Glendinning, S. N. Dixit, B. A. Hammel, D. H. Kalantar, M. H. Key, J. D. Kilkenny, J. P. Knauer, D. M. Pennington, B. A. Remington, R. J. Wallace, and S. V. Weber, Phys. Rev. Lett. **78**, 3318 (1997).
6. R. H. Lehmberg, A. J. Schmitt, and S. E. Bodner, J. Appl. Phys. **62**, 2680 (1987).
7. S. Skupsky, R. W. Short, T. Kessler, R. S. Craxton, S. Letzring, and J. M. Soures, J. Appl. Phys. **66**, 3456 (1989).
8. H. Takabe *et al*., Phys. Fluids **28**, 3676 (1985).
9. R. Betti, V. N. Goncharov, R. L. McCrory, P. Sorotokin, and C. P. Verdon, Phys. Plasmas **3**, 2122 (1996).
10. M. Honda and K. Mima, to be published in Physical Review Letters.
11. Y. Lin, T. J. Kessler, and G. N. Lawrence, Opt. Lett. **20**, 764 (1995).
12. D. K. Bradley, T. Boehly, D. L. Brown, J. Delettrez, W. Seka, and D. Smith, in *Laser Interaction and Related Plasma Phenomena*, edited by H. Hora and G. Miley (Plenum Press, New York, 1991), Vol. 9, pp. 323–334.
13. O. L. Landen, P. M. Bell, J. A. Oertel, J. J. Satariano, and D. K. Bradley, in *Ultrahigh- and High-Speed Photography, Videography, and Photonics '93*, edited by P. W. Roehrenbeck (SPIE, Bellingham, WA, 1993), Vol. 2002, pp. 2–13.
14. T. R. Boehly, D. D. Meyerhofer, J. P. Knauer, D. K. Bradley, R. L. Keck, V. A. Smalyuk, W. Seka, and C. P. Verdon, "Laser-Imprinting Studies on the OMEGA Laser System," to be published in the *Proceedings of the Thirteenth International Conference on Laser Interactions and Related Plasma Phenomena (LIRPP)*, Monterey, CA, 13–18 April 1997.